NASA TECHNICAL NOTE

NASA TN D-5218

NASA TN D-5218

CONCEPTUAL STUDY OF ROCKET-SCRAMJET HYBRID ENGINES IN A LIFTING REUSABLE SECOND STAGE

by Andrzej Dobrowolski and John L. Allen

Lewis Research Center
Cleveland, Ohio

NATIONAL AERONAUTICS AND SPACE ADMINISTRATION • WASHINGTON, D. C. • MAY 1969

CONCEPTUAL STUDY OF ROCKET-SCRAMJET HYBRID ENGINES IN A LIFTING REUSABLE SECOND STAGE

By Andrzej Dobrowolski and John L. Allen

Lewis Research Center
Cleveland, Ohio

NATIONAL AERONAUTICS AND SPACE ADMINISTRATION

For sale by the Clearinghouse for Federal Scientific and Technical Information
Springfield, Virginia 22151 – CFSTI price $3.00

ABSTRACT

A simplified analysis of a prismatic-delta configuration flying a near minimum fuel consumption path from staging to orbit showed relative advantages for air-augmented propulsion systems. The trajectory had a constant product of pressure and Mach number during powered flight which extended to speeds slightly greater than orbital so that a zoom maneuver could be used to obtain final orbital altitude. For staging at Mach 10, the estimated payload fraction (payload to staging weight) for the best air-augmented case (3:1 ratio of air to rocket flow) was $1\frac{1}{2}$ times better than that using pure rocket power and $7\frac{1}{2}$ times better than that using pure scramjet power.

CONCEPTUAL STUDY OF ROCKET-SCRAMJET HYBRID ENGINES IN A LIFTING REUSABLE SECOND STAGE

by Andrzej Dobrowolski and John L. Allen

Lewis Research Center

SUMMARY

The lifting second stage of a reusable orbital booster is analyzed employing a highly simplified approach so that major problems, trade-offs, and potential can be identified. The powerplant is a hydrogen-oxygen rocket with various degrees of air augmentation ranging from zero for the pure rocket to infinity for the pure scramjet. Additional hydrogen is injected to allow stoichiometric combustion of the air. A trajectory characterized by a constant product of pressure and Mach number is flown during powered flight to speeds slightly above orbital so that a zoom maneuver can be used to obtain the final 100-mile (1.6×10^5-m) orbit.

The vehicle configuration was a prismatic delta (flat-top wedge with triangular cross section). A strong interdependence is shown between propulsive, aerodynamic, and structural characteristics. For a staging Mach number of 10 and the same trajectory, the estimated ratio of payload to staging weight for the best air-augmented case (3:1 ratio of air to rocket flow) was $1\frac{1}{2}$ times better than pure rocket power and $7\frac{1}{2}$ times better than that for pure scramjet power.

INTRODUCTION

Relatively little attention has been given to the study of second stages on a lifting trajectory powered by some form of air-breathing propulsion. There have been many concepts proposed for reusable first stages, ranging from rockets through a perplexing variety of air-breathing systems (see, for example, ref. 1). The second stage in accelerating from, say, 50 to 100 percent of orbital velocity must supply about 75 percent of the orbital energy and, therefore, would seem to justify further study. For either the first or upper stages, the provision of some lift capability in the form of wings or body shaping gives a controlled landing ability for easy recovery, subsequent reuse, and in-

creased flexibility of launch operations. If this added aerodynamic lift capability is designed for use during ascent as well as recovery, then flatter ascent trajectories in the denser, lower altitudes would be favored at the expense of increased structural weight. For such trajectories, the advantages of increased specific impulse, but greater weight, promised by some forms of air-breathing or air-augmented powerplants can be assessed as well as pure rocket propulsion.

Most studies of reusable second stages have considered only rocket or scramjet propulsion. In reference 2, the scramjet powered reusable second stage was found to be relatively unattractive compared with a rocket-powered stage. The present study considers a spectrum of powerplants ranging from the pure rocket at one extreme to the scramjet at the other extreme with the accompanying air-augmentation ratio varying from zero to infinity (air-augmentation ratio is defined as the weight of air flow, supplied by an inlet, divided by the weight of rocket propellent flow). Within this spectrum are hybrid rocket-scramjet engines with finite values of air-augmentation ratio and values of specific impulse, thrust coefficient, and engine weight intermediate between those of the pure rocket and the pure scramjet. Proper choice of air-augmentation ratio for the vehicle configuration and trajectory is one of the main problems of the study.

The fixed geometry hybrid engine postulated is composed of a primary rocket component and a secondary scramjet component that includes an inlet, mixer, burner, and nozzle. The primary rocket burns hydrogen and oxygen in a stoichiometric mixture ratio. The rocket flow is fully mixed with the supersonic air before additional hydrogen is added to complete the combustion of the mixture.

The propulsive, aerodynamic, and structural characteristics of the vehicle are shown to be strongly interrelated. Within the framework of the analysis the following important factors are related by the parameters of body volume to planform area ($V^{2/3}/S$) and span to length (b/c):

(1) Lift-drag ratio affects the required thrust.

(2) Skin wetted area affects the insulation weight.

(3) Inlet capture area affects the air mass flow available for propulsion.

The lifting trajectory derived herein is characterized by a schedule such that the product of atmospheric pressure and Mach number is constant. This trajectory gives approximately minimum fuel consumption and a constant mass flow per unit area which greatly simplifies the analysis.

In this study, the optimum payload configuration can be identified for a given staging Mach number in terms of air-augmentation ratio, vehicle geometry, and flight path. The payload was selected to be 25 000 pounds (11 340 kg). Staging Mach numbers between 8 and 12 are investigated. The criterion of merit postulated is the minimum gross weight of the second stage of the orbital booster. No consideration is given in the present study to the launch vehicle that propels the second stage to its initial flight condition.

A highly simplified method of calculation based on idealized component characteristics is employed in this study. It is believed that this simple gross analysis yields useful results that are not obscured by excessive details. Moreover, any detailed analysis of reuseable second stages would be weakened by the fact that all of the required technologies currently are too poorly developed for accurate evaluation.

ANALYSIS AND RESULTS

The following parameters have been found to be useful in relating the propulsion, aerodynamic, structural, and trajectory characteristics of a reuseable second stage vehicle. A major goal of the study was to identify the optimum values:

$V^{2/3}/S$ volume-surface parameter (It dictates the L/D capability of the vehicle, the engine capture area A_{oo}, and the skin area S_{oa} (symbols are defined in appendix G).)

pM means of specifying the flight trajectory (It dictates the air mass flow through the engine capture area A_{oo} and influences the structural weight.)

$\overline{m}$ air-augmentation ratio (It dictates the specific impulse and the thrust of the stage.)

Engine Model

The hybrid engine incorporates both air-breathing and rocket components as shown in figure 1. Combined with the air induction system is a hydrogen-oxygen rocket operating stoichiometrically (to prevent combustion in the mixer) as opposed to the normal fuel-rich operation of the usual rocket. Both the inlet and the primary rocket are of

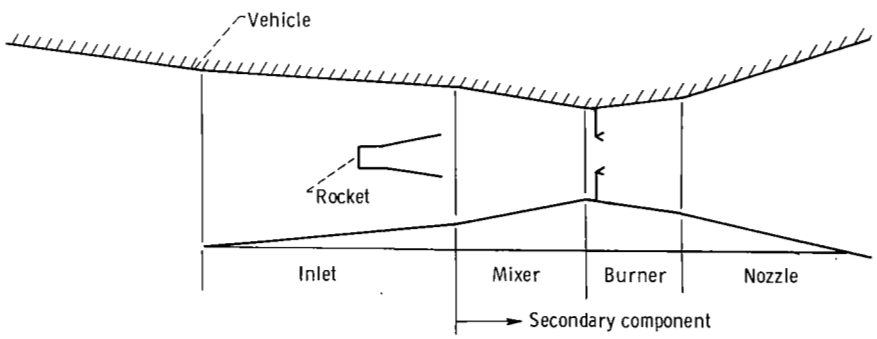

Figure 1. - Schematic of rocket-scramjet hybrid engine.

fixed geometry. A combustion pressure of 1000 psi (6.89×10^6 N/m^2) is assumed for the rocket.

The air-breathing component of the hybrid engine, usually referred to as the secondary component, is selected by matching the inlet, mixer, and burner according to specific interface requirements, as discussed later (see Powerplant Performance, p. 13). Downstream of the rocket-inlet combination is a section to allow complete mixing of the inducted supersonic air with the primary jet. Additional fuel is supplied to complete the stoichiometric combustion of the air in the burner section. Burning occurs at supersonic speeds. A fixed-geometry nozzle is integrated into the vehicle boattail.

Vehicle Configuration

The vehicle configuration used in this study is a wingless lifting body. As shown in figure 2, it is idealized as a flat-top wedge with a triangular cross section and is referred to in this report as a prismatic delta. Such a configuration is easily amenable to simplified aerodynamic and structural analysis and was adopted because the calculated weight and aerodynamic characteristics were found to be comparable with those of more realistic configurations studied by others.

If this type of vehicle were to be built, it would have an upper surface shaped to aid the subsonic lift-drag ratio which should exceed a value of 5. Vertical stabilizers located at the tips of the delta planform would provide lateral stability. Auxiliary turbojet power would be used during subsonic maneuvers and to assist during the horizontal airplane-type landing. Figure 2 indicates that the usual components of the aircraft are

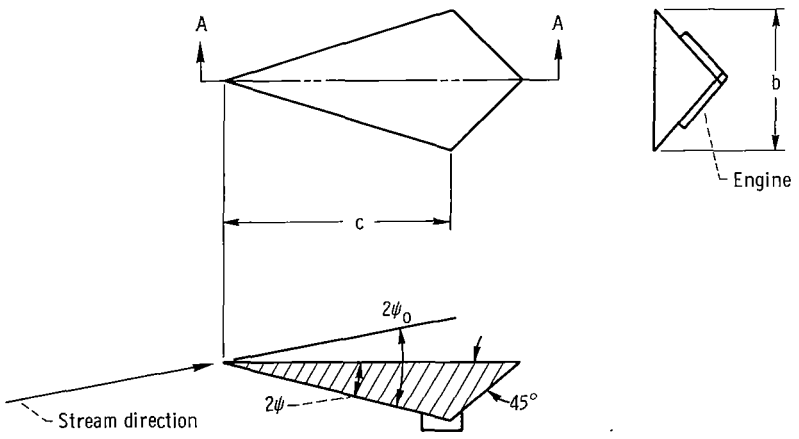

Section A-A

Figure 2. - Vehicle configuration.

integrated for generating lift, providing volume, and acting as portions of the engine inlet and exhaust nozzle.

In the present study, two fundamental design constraints affected the inlet size: (1) the engine inlet (when other than the pure rocket case) is located entirely within the pressure field on the lower side of the vehicle, and (2) the capture area is arbitrarily limited to that portion of the vehicle cross section below the plane or axis that defines the zero net lift attitude (see appendix E). This constraint is based on the practical consideration that installation of a hybrid engine near the tip regions would be difficult. Some other assumption would very likely give a different combination of volume-surface area, trajectory, and air-augmentation parameters for best payload.

Trajectory

The trajectory traversed will have a strong influence on the problem of matching the powerplant and structure to the vehicle geometry for maximum payload. Inasmuch as a lifting trajectory is specified, the powered portion will terminate at an altitude considerably less than the goal of a 100-mile (1.6×10^5-m) orbit. Consequently, a velocity greater than orbital will be needed during powered flight so that a zoom maneuver can be used to attain the desired orbital altitude.

The path followed during powered flight is characterized by a constant product of ambient pressure and flight Mach number (pM). This results in approximately constant air flow through the engine, and because of the assumption of stoichiometric combustion, the fuel flow rate is likewise constant.

This trajectory (pM = constant) is a close approximation to the path $\cdot pM^{4/3}$ = constant shown in appendix A to give minimum fuel consumption over a considerable portion of the desired velocity increment. Near orbital velocity the path angle required by the optimum solution becomes excessive and finally indeterminate.

Figure 3 shows several pM = constant paths within altitudes of 50 000 to 200 000 feet (15 230 to 60 900 m) and includes one case of the more optimum $pM^{4/3}$ = constant path (extended beyond the applicable velocity). Also, several constant dynamic pressure (pM^2 = constant) paths frequently proposed in air-breathing propulsion analyses are shown to be quite different from the other two examples. Lines of constant skin temperature 1 foot (1/3 m) aft of the leading edge of a flat plate at zero angle of attack are superimposed.

The five phases of the reusable second stage flight are as follows (see fig. 4):

(1) Separation from the launch vehicle at a given Mach number M_s, a given altitude h, and a path angle compatible with pM = constant flight

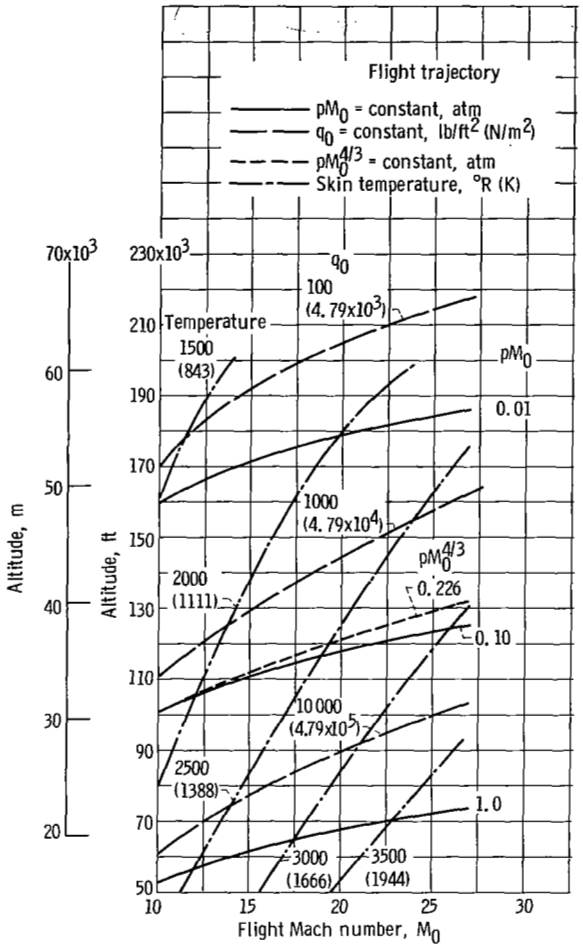

Figure 3. - Typical flight trajectories.

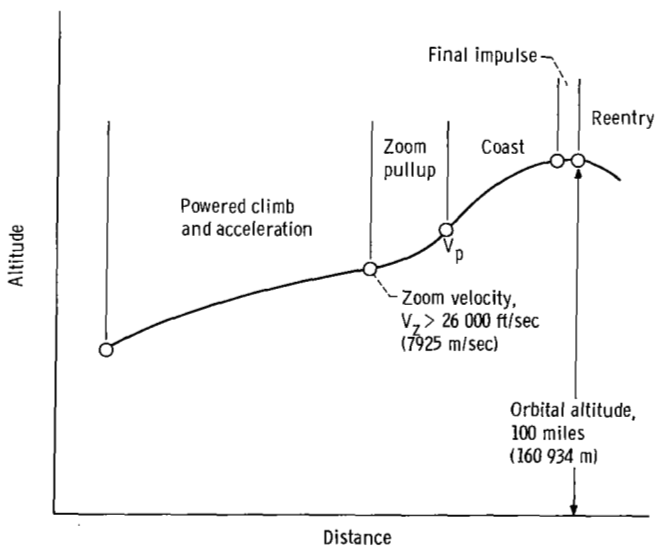

Figure 4. - Schematic of complete flight path.

(2) An acceleration-climb path along the pM = constant trajectory culminating in a zoom velocity V_z greater than the orbital velocity V_r

(3) A zoom maneuver to achieve an altitude of 100 miles (1.6×10^5 m) at the velocity V_r (The zoom consists of a pullup in the atmosphere with an initial velocity V_z and then a ballistic path tangential at its peak to the 100-mile (1.6×10^5 m) orbit, where the final small impulse is applied.)

(4) Separation or unloading of the payload

(5) Retroimpulse and glide reentry of the vehicle terminated by the approach and landing with the help of turbojets

Each of the flight paths is explored with a series of different geometry vehicles represented by the volume-surface parameter $V^{2/3}/S$. This parameter defines the L/D capability of the vehicle (see Vehicle Aerodynamics, p. 16); hence, it dictates the required magnitude of the zoom velocity. For a given L/D, there is a corresponding zoom velocity V_z and pullup angle. For a large L/D, V_z is moderate; for a small L/D, V_z becomes excessive. This is shown in figure 5. (See also appendix B for the derivation of V_z.) Thus, a small L/D vehicle will have a protracted powered flight. Each vehicle on a given pM = constant path is investigated for a series of engines with different augmentation ratios $\overline{m}$.

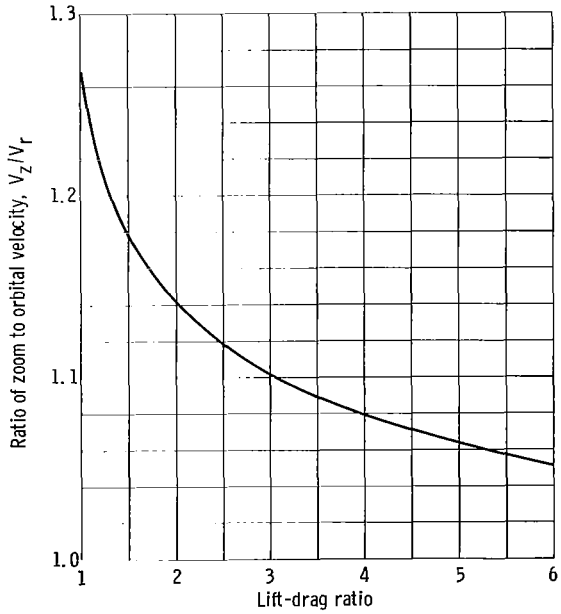

Figure 5. - Relation of lift-drag ratio and zoom-orbital velocity ratio necessary to attain an orbital altitude of 100 miles (160 934 m).

Powerplant Performance

At high Mach number flight the shock envelope formed is very close to the surfaces of the vehicle. The deflection of the flow passing through the oblique shock can be calculated from the well-known equation relating wave angle β and deflecting angle α (flat-plate angle of attack):

$$\frac{\tan(\beta - \alpha)}{\tan \beta} = \frac{(\gamma - 1)M^2 \sin^2\beta + 2}{(\gamma + 1)M^2 \sin^2\beta}$$

This can be put in the form

$$\frac{\tan(\beta - \alpha)}{\tan \beta} = \frac{(\gamma - 1) + \dfrac{2}{M^2 \sin^2\beta}}{(\gamma + 1)}$$

Using small angle approximations reduces the relation to the following approximation between wave and deflection angle:

$$\beta = \left(\frac{\gamma + 1}{2}\right)\alpha \pm \sqrt{\left[\left(\frac{\gamma + 1}{2}\right)\alpha\right]^2 + \frac{4}{M^2}} \tag{1}$$

As $1/M^2 \to 0$,

$$\beta \to \left(\frac{\gamma + 1}{2}\right)\alpha$$

Thus, it is seen that at these very high speeds the shock wave angle is only slightly larger than the surface angle of the vehicle and is not a strong function of Mach number.

The engine inlet is located on the underside of the vehicle within the shock envelope. The size of the inlet is reduced by using the vehicle forebody as a precompression surface. The area of the captured stream tube of air does not change appreciably with angle of attack in the hypersonic region.

The powerplant performance was calculated for hydrogen fuel by the methods of references 3 and 4 assuming chemically frozen exhaust nozzle expansion. The overall stagnation pressure ratios of the combined inlet, mixer, and burner of various geometries were determined along several pM = constant paths and for a range of air-augmentation ratios. The variation of engine performance with the change in vehicle angle of attack along the flight path was considered beyond the broad concepts of this re-

port. From equation (41) of reference 4,

$$I_s = \frac{(\overline{m} + 1)V_3 - \overline{m}V_o}{g\left(1 + \overline{m}\frac{f}{a}\right)} \tag{2}$$

and

$$C_F = \frac{f}{a}\frac{m_1}{A_{oo}}\frac{I_s}{q} \tag{3}$$

Figure 6 shows specific impulse I_s against specific thrust coefficient C_F plotted for flight Mach numbers M_o of 10, 17, and 25 for a number of selected augmentation ratios. The figure is plotted for an equivalence ratio of 1. The variation of the specific impulse for air-augmentation ratio of $\overline{m} = 3$ is shown in figure 7 against the equivalence ratio of the fuel in the burning duct aft of the mixing duct. There is a marked increase of the specific impulse with the increase of the equivalence ratio up to its stoichiometric value. At equivalence ratios higher than 1, the increase in specific impulse and thrust coefficient is slight. All vehicle performance calculations used engine performance data at an equivalence ratio of 1.0.

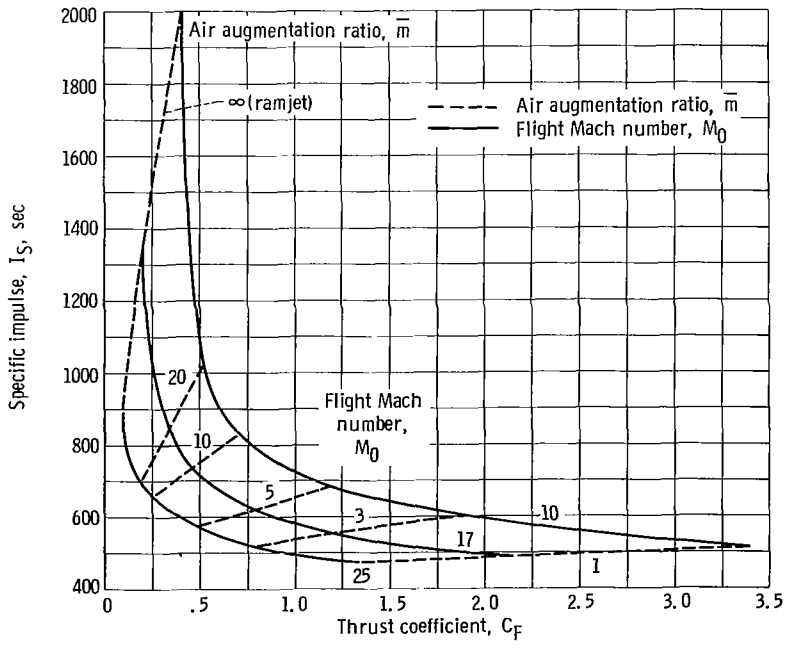

Figure 6. - Performance of the hybrid engine. Altitude, 150 000 feet (45 720 m); equivalence ratio, 1.0.

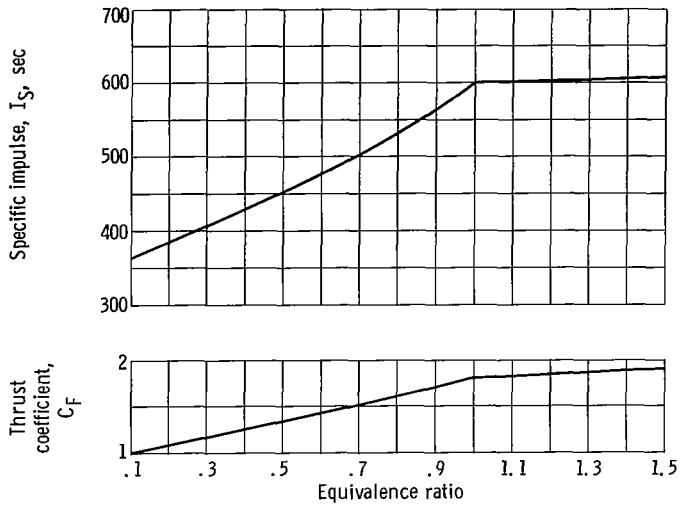

Figure 7. - Effect of equivalence ratio on hybrid engine performance. Flight Mach number, 10; altitude, 150 000 feet (45 720 m); air-augmentation ratio, 3.

Hybridization

The nominal propulsion system studied herein is a hybrid; that is, the rocket exhaust has been submerged in a secondary airflow in a ducted rocket arrangement. This increases specific impulse and thrust due to the exchange of thermal and kinetic energy. Further increases in thrust and impulse may be obtained by the subsequent addition of heat to the mixed flow. An alternative arrangement without the ejector effect would be the simultaneous but separate use of selected sizes of rocket and scramjet. It is shown in appendix C that the general merits of hybridization, as determined from total enthalpy considerations, are minimal in the hypersonic region (differences in engine weights are neglected). A sample comparison at a Mach number of 10, altitude of 150 000 feet (45 720 m), and an equivalence ratio of 1.0 is shown in table I.

Although these differences appear worthwhile, at higher speeds the benefit of hybridization diminishes as shown in appendix C. Hence, the rocket-scramjet hybrid considered here has similar performance to a set of a separate rocket and scramjet; the results presented here in terms of hybrids can be interpreted equally well in terms of a separate rocket and scramjet, neglecting differences in engine weights. The magnitude of the air-augmentation ratio of the single-duct concept can be translated into relative sizes of rocket and scramjet in the two-ducted concept.

TABLE I. - EXAMPLES OF HYBRID AND

SEPARATE POWERPLANTS

[Flight Mach number, 10.]

Powerplant	Air-augmentation ratio, $\overline{m}$	Thrust coefficient, C_F	Specific impulse, I_S, sec
Hybrid	3	1.9	600
Separate	3	1.4	570
Hybrid	10	.7	820
Separate	10	.6	720

Vehicle Aerodynamics

The two fundamental parameters involving the shape of the configuration that affect the aerodynamic characteristics of a hypersonic vehicle are the volume-surface parameter $V^{2/3}/S$ and the span-length ratio b/c. The lift-drag ratio L/D is often shown as a function of $V^{2/3}/S$ and b/c as described in reference 5. Similar trends of L/D for the prismatic-delta vehicle used herein are shown in figure 8 and were determined by the methods given in appendix D. These two parameters are conveniently related to the vehicle's wedge angle by the expression

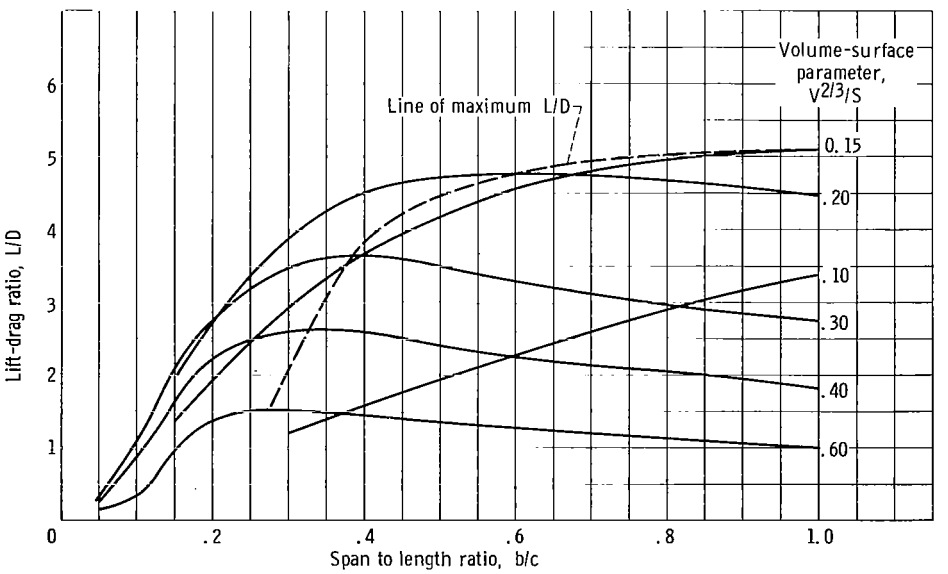

Figure 8. - Effect of vehicle geometry on lift-drag ratio.

$$\frac{V^{2/3}}{S}\left(\frac{b}{c}\right)^{1/3} = \left(\frac{2\sqrt{2}}{3}\psi\right)^{2/3} \tag{4}$$

Thus, for large volume-surface parameters $V^{2/3}/S$, high values of b/c correspond to large vertex and wedge angles which give greater nonfriction drag losses. Alternately, for the same $V^{2/3}/S$, b/c must be small for thin vehicles (small ψ); however, the contribution from skin friction increases. Therefore, the lift-drag ratio reaches a maximum for some optimum span-length ratio for each value of volume-surface parameter.

The resulting variation of maximum lift-drag ratio with volume-surface parameter is shown in figure 9 and was the basis for subsequent results which correspond in all cases to optimum span-length ratio. The wedge angle of the vehicle 2ψ for optimum span-length ratio varied from about 7° to 30° over the range of $V^{2/3}/S$ from 0.1 to 0.6. Other hypersonic vehicle shapes such as elliptic or half cones, etc. often considered have $V^{2/3}/S$ in the 0.10 to 0.20 range, which indicates a lift-drag ratio capability between 5.5 and 4.5 (ref. 6). (By way of conceptual interpretation, for a cube, $V^{2/3}/S = 1.0$, and for a square flat plate of thickness t_1, $V^{2/3}/S = (t_1/c)^{2/3}$ - a very small number.) Since a small value of $V^{2/3}/S$ implies a large wetted surface and, hence, a significant weight penalty due to the heavy thermal protection required for hypersonic vehicles, the detailed design should consider the trade-offs involved at off-optimum lift-drag ratios. This was not attempted in the present study.

The relation between skin area and planform (surface) area parameters for optimum span-length ratio is shown in figure 10. For $V^{2/3}/S < 0.30$ where lift-drag ratios are increasing (fig. 9), the total outside skin area is increasing for any given volume; hence, the thermal protection penalty will be greater.

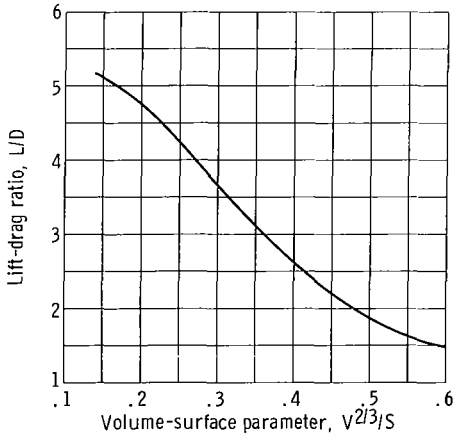

Figure 9. - Effect of volume-surface parameters; optimum span-length ratio.

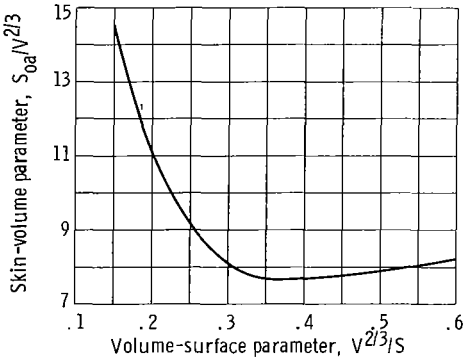

Figure 10. - Relation between skin area and planform area parameters; optimum span-length ratio.

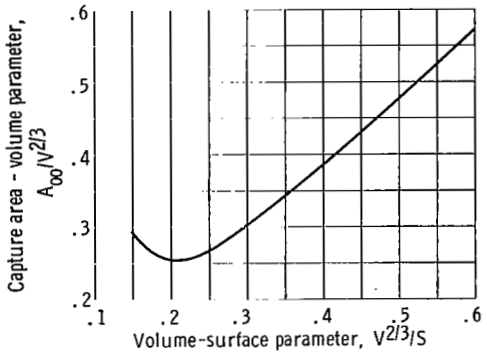

Figure 11. - Relation between capture area and planform area parameters; optimum span-length ratio.

In a similar manner, figure 11 shows the dependence of capture area on planform area for optimum span-length ratios. The capture area is determined by the zero lift condition as explained in appendixes D and F. Capture area is increasing for $V^{2/3}/S > 0.2$ where skin area is near minimum (fig. 10) and lift-drag ratios are smaller (fig. 9). Thus, specifying the volume-surface parameters not only gives a maximum lift-drag ratio but also establishes the maximum air mass flow available for propulsion. In an alternate form of interpretation the ratio of capture to planform areas, A_{00}/S, varies from about 0.035 to 0.32 over the range of $V^{2/3}/S$ from 0.1 to 0.6 for optimum span-length ratio.

To interpret the preceding general results in the framework of the second-stage booster problem, it must be assumed that the vehicle with a superior maximum L/D will maintain a relative advantage throughout the staging to orbit speed range. In other words, over the flight path from staging to orbit the maximum lift-drag ratio occurs at only one velocity since aerodynamic lift diminishes as centrifugal lift increases. The maximum thrust requirement occurs at staging where the lift and, consequently, the induced drag are maximum.

Structural Analysis

In contrast to the usual nonlifting rocket trajectory, the path of the air-breathing vehicle results in an environment of higher pressures and temperatures for a longer time. Therefore, the air breather will be penalized by generally higher component weights and dissipation of the large heat input is a major problem. Heat protection by radiation is assumed utilizing, as required by maximum temperature, superalloy heat shields or refractory metal heat shields with oxidation protecting coatings and special

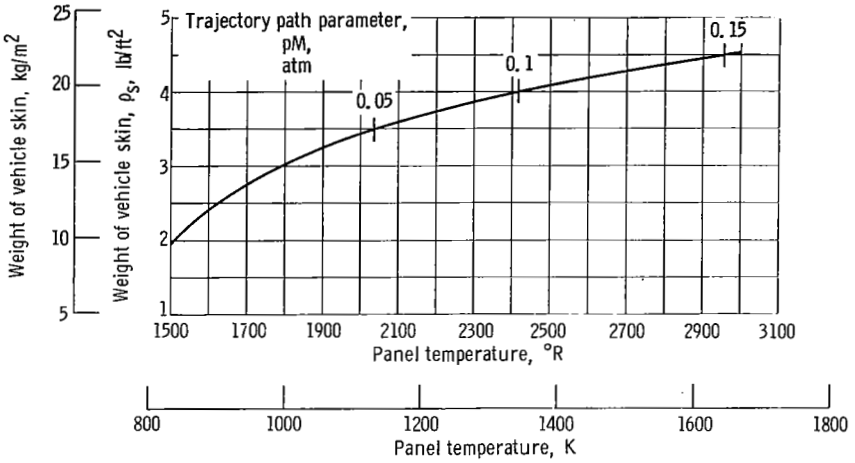

Figure 12. - Variation of assumed skin weight per unit area with temperature.

underside insulation. Corresponding estimates of the thermal protection system weight, referred to hereinafter as skin, are shown in figure 12 as a function of panel surface temperature. The curve is based on the data of references 7 and 8. Determining a representative skin temperature for the entire vehicle is, of course, a complex and elaborate procedure far beyond the scope of this report. The unit skin weights selected for vehicles designed for three different path parameters pM are designated in the figure.

In the stringent thermal environment, a semimonocoque structure cannot be used and the aerodynamic loading will have to be supported by an internal trusswork. Figure 13 shows the variation of the weight of the trusswork per cubic foot of enclosed

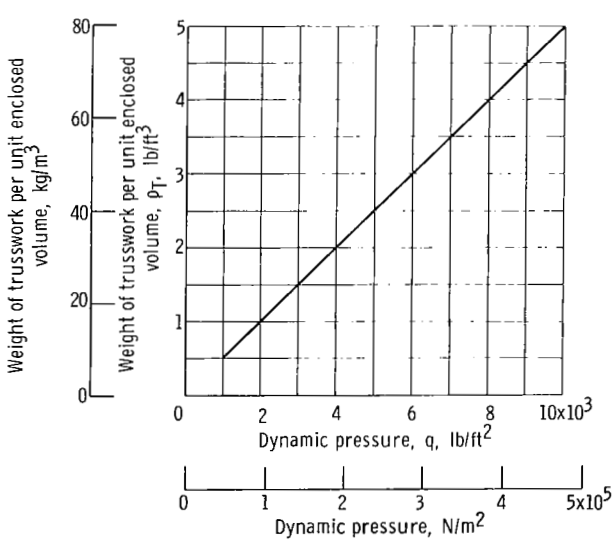

Figure 13. - Effect of dynamic pressure on trusswork weight per unit volume.

volume against the flight dynamic pressure. A typical value will be around 1.5 pounds per cubic foot (24 kg/m^3). The preliminary structural analysis is contained in appendix E.

The weight of the tankage was taken as 1.0 pound per cubic foot (16 kg/m^3). The weight of the air-breathing component of the engine is assumed to be 50 pounds per square foot (244 kg/m^2) of capture area, and the rocket's weight is 2 percent of its thrust.

If a typical value of the weight of skin per square foot of 4 pounds (19.5 kg/m^2) is assumed for a $V^{2/3}/S = 0.30$ vehicle, the variation of the weight of skin per unit volume enclosed is shown in figure 14. It is seen that on a volume basis the weight of this component is comparable to that for the tanks or the truss.

Hence, the structural weight of this type of vehicle ($V^{2/3}/S = 0.30$) can be expected to be of the order of 5 pounds per cubic foot (80 kg/m^3) enclosed. This can be compared with the propellant densities given in table II. (Propellant density varies with air-augmentation ratio because of the fuel needed to complete the combustion of all the captured air.)

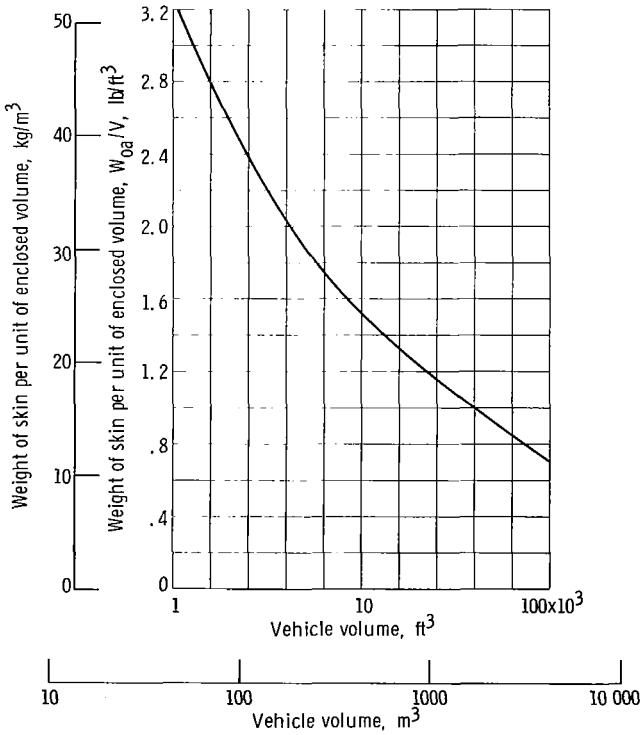

Figure 14. - Effect of vehicle volume on unit skin weight. Volume-surface parameter, $V^{2/3}/S$, 0.30; skin weight, 4 pounds per square foot (19.5 kg/m^2).

TABLE II. - VARIATION OF PROPELLANT DENSITY WITH AIR-AUGMENTATION RATIO

[Equivalence ratio, 1.0.]

Air-augmentation ratio, $\overline{m}$					
0	1	3	5	10	∞
Propellant density, ρ_f, lb/ft^3 (kg/m^3)					
26.4 (422.8)	23 (352.3)	18.7 (299.4)	16 (256.2)	12.4 (198.6)	4.4 (70.45)

Stage Performance

The overall performance of the vehicle in its function as a booster stage and as measured by the payload ratio is investigated by selecting several paths (pM = constant) and a given geometry vehicle, dictated by a specific value of $V^{2/3}/S$. The secondary flow and its amount is dictated by the geometry and trajectory of the vehicle. The option that remains is the amount of the primary flow which is determined by the parametric choice of $\overline{m}$. The larger this primary flow, the smaller the specific impulse and the greater the thrust. Further explanation of the calculation procedure is given in appendix F. The payload fractions presented hereinafter are primarily intended for relative comparison of the propulsion systems studied rather than absolute predictions. A variety of air-augmentation ratios have been examined resulting in figures 15 and 16 where the optimum vehicle and the path have been identified from a large number investigated. The greatest payload ratio obtained is for the vehicle $V^{2/3}/S = 0.30$, the path pM = 0.10 atmosphere, and it is relatively insensitive to an air-augmentation ratio between values of 3 and 6. This payload ratio P/W_o is equal to 0.11 for a staging Mach number M_s of 10, as seen from figure 15. For the same flight path, the corresponding pure rocket stage value is $P/W_o = 0.07$, and the corresponding scramjet stage value is 0.015. In the case of the pure rocket, the payload ratio is practically independent of the type of vehicle used. In the case of the scramjet, the only vehicle that could attain some positive performance had a high L/D with $V^{2/3}/S = 0.15$. Even then, the velocity reached on pure scramjet power was only 23 000 feet per second (7010 m/sec); the remaining acceleration had to be completed by rocket. In the region of maximum payload the lower value of air-augmentation ratio of 3 was chosen for further illustration. The hypothesis was that in an actual design some effects not considered herein, such as mixing and entrainment losses, would favor the smaller value of augmentation ratio.

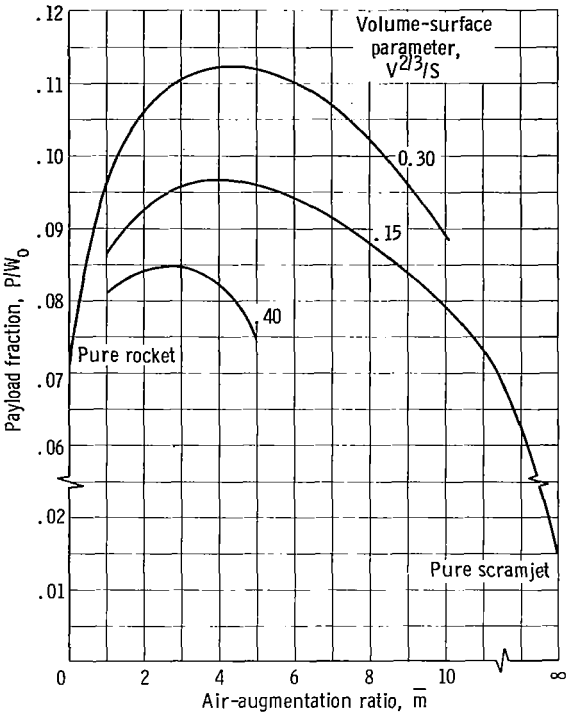

Figure 15. - Variation of payload fraction with air-augmentation ratio and volume-surface parameter. Staging Mach number, 10; trajectory parameter, pM, 0.10 atmosphere.

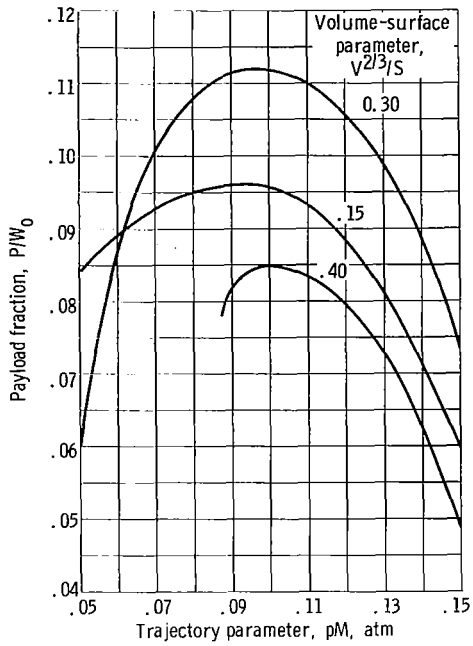

Figure 16. - Variation of payload ratio with trajectory parameter pM. Staging Mach number, 10; air-augmentation ratio, 3.

The results in figure 15 are for only a single path, pM = 0.10 atmosphere, which requires a powered climb between 100 000 and 130 000 feet (30 500 to 39 600 m) in altitude (see fig. 3). Figure 16 shows the performance of hybrid vehicles having an air-augmentation ratio $\overline{m} = 3$ for various values of the path parameter pM and vehicle volume-surface parameters. It is seen that at higher altitudes (pM < 0.06 atm) a $V^{2/3}/S = 0.15$ vehicle is better; however, over most of the paths, the $V^{2/3}/S = 0.30$ vehicle that combines a moderate L/D capability with low values of skin-volume $S_{oa}/V^{2/3}$ parameter and acceptable capture area - volume parameter $A_{oo}/V^{2/3}$ is superior. The specific component weights for the rocket, the optimum hybrid, and the scramjet stages are given in table III. The best hybrid included is $V^{2/3}/S = 0.30$, $\overline{m} = 3$, and pM = 0.10 atmosphere. It will be observed that there is a great variation in the volume of the vehicle depending on the type of the engine. The hybrid stage is only half the size of the rocket stage and an order of magnitude smaller than the scramjet stage. To help visualize the differences, figure 17 shows the three optimum vehicles - scramjet, rocket, and hybrid (rocket-scramjet) - drawn to scale. The size of the vehicle is reduced drastically when rockets are incorporated into the propulsion system. Thus, the estimated benefit accrued by utilizing hybrid rather than rocket

TABLE III. - COMPARISON OF WEIGHT DISTRIBUTIONS AND VOLUME PARAMETERS FOR ROCKET-, HYBRID-, AND SCRAMJET-POWERED VEHICLES

[Trajectory parameter, pM = 0.1 atm.]

(a) Weight distributions

Component	Rocket	Hybrid ($\overline{m}$ = 3)	Scramjet	Rocket	Hybrid ($\overline{m}$ = 3)	Scramjet
	Weight distribution					
	lb			kg		
Payload	25×10^3	25×10^3	25×10^3	11.34×10^3	11.34×10^3	11.34×10^3
Tanks	16	9.6	180	7.25	4.355	81.6
Truss	24	14.4	270	10.88	6.53	122.4
Skin	15.5	12.8	162	7.03	5.8	73.45
Engine	7	9.2	41	3.17	4.17	18.6
Landing equipment (landing gear, return engine and fuel, orbital impulse rocket	12.5	9.2	131	5.67	4.17	59.4
Fuel and oxidizer	257	144.8	851	116.5	65.7	356
Total stage weight, W_o	357	225	1660	162	102	752.8

(b) Volume parameters

Parameter	Rocket	Hybrid ($\overline{m}$ = 3)	Scramjet
Total volume, ft^3 (m^3)	16×10^3 (453)	9.6×10^3 (271.8)	180×10^3 (509.5)
Volume-surface parameter, $V^{2/3}/S$	0.3	0.3	0.15

propulsion is approximately 60 percent in payload fraction when the integrated aspects of vehicle geometry, trajectory, and air-augmentation ratio are considered.

It is expected that the payload ratio will vary directly with staging Mach number. This is illustrated by figure 18 which shows staging Mach numbers from 8 to 12 for the optimum configuration and trajectory. Selection of the best staging Mach number requires consideration of the first stage also; however, this is beyond the scope of the present study.

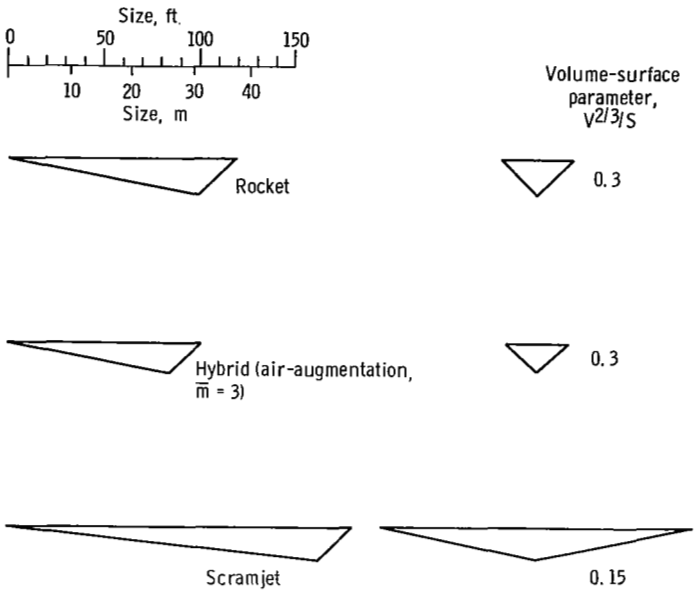

Figure 17. - Relative sizes of vehicles using different propulsion systems. Payload, 25 000 pounds (11 340 kg); optimum span-length ratio, staging Mach number, 10; trajectory parameter, pM, 0.1 atmosphere.

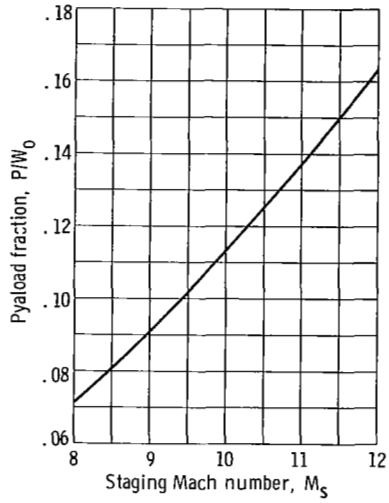

Figure 18. - Dependence of payload fraction on staging Mach number. Volume-surface parameter, $V^{2/3}/S$, 0.30; air-augmentation ratio, 3; trajectory parameter, pM, 0.10 atmosphere.

CONCLUDING REMARKS

A conceptual study was made of a lifting reuseable second stage using rocket-scramjet propulsion. The hybrid engine has a hydrogen-oxygen rocket with varying degrees of air augmentation extending from the pure rocket to the pure scramjet with stoichiometric combustion in all cases. The adopted trajectory closely resembles the optimum minimum fuel consumption path where possible. The trajectory was characterized by a constant product of ambient pressure and Mach number which gave a nearly constant air mass flow rate. Powered flight extended beyond orbital velocity, depending on the maximum lift-drag capability of the vehicle, so that a zoom maneuver could be used to attain the final orbit altitude of 100 miles (1.6×10^5 m).

The vehicle geometry was assumed to be a prismatic delta (flat-top wedge with triangular cross section). A strong relation was found between the powerplant type and vehicle geometry. Span-length ratios were chosen to give maximum lift-drag ratios for each value of the volume-surface area parameter $V^{2/3}/S$. For the lower values of $V^{2/3}/S$ usually suggested for hypersonic vehicles (0.1 to 0.2), the lift-drag ratios are highest (4.5 to 5.5), but available capture area (stream tube precompressed by the bottom surface of the vehicle) is smallest and skin area (needing thermal protection) is largest. For high values of $V^{2/3}/S$ (0.5), the lift-drag ratio is low (<2.0), but capture area is highest and skin area is low. Thus, the capture area attainable affects the

powerplant selection (air-augmentation ratio) and coupled with the constraint of sufficient propellant volume determines the ability to attain orbital flight. The payload placed in orbit, however, depends on the vehicle size and the empty weight (structure, engine, and equipment).

Because of the high temperature environment, a pin-jointed trusswork with an insulating skin was selected for the structure. For the best vehicle, the weight of the truss per unit volume supported was comparable to those for the skin and propellant tanks, the sum of which was approximately 5 pounds per cubic foot (80 kg/m^3). This compares with propellant density requirements of 26.4 pounds per cubic foot (422.8 kg/m^3) for the rocket only case, 18.7 pounds per cubic foot (299.4 kg/m^3) for an air-augmentation ratio of 3, and 4.4 pounds per cubic foot (70.45 kg/m^3) for the scramjet only case (hydrogen is the only fuel considered).

The vehicle having the highest estimated payload to staging weight ratio was characterized by a volume-surface parameter $V^{2/3}/S$ of 0.3 (span-length ratio of 0.385), an air-augmentation ratio of 3, a maximum lift-drag ratio of 3.6, and a trajectory path of pressure times Mach number = 0.1 atmosphere. For a staging Mach number of 10, the estimated payload fraction for the second stage using air-augmented propulsion was $1\frac{1}{2}$ times better than using pure rocket power. For the scramjet case on the same trajectory, the best volume-surface parameter was 0.15 (higher L/D), but the payload fraction was only 14 percent of that for the air-augmentation case.

Thus, a rocket-scramjet propulsion system, whether hybrid or not, was found to promise payload capabilities superior to those attainable with a rocket or scramjet alone (on the same trajectory). Achieving this promise requires an integrated consideration of the vehicle geometry, trajectory, and powerplant. These results are, of course, dependent on the assumptions and simplified analysis used to identify some of the major problems and trade-offs involved. Also, other important factors, such as development cost, risk, availability, and complexity must, in the end, be considered.

Lewis Research Center,
National Aeronautics and Space Administration,
Cleveland, Ohio, May 24, 1968,
789-30-01-01-22.

APPENDIX A

OPTIMUM ASCENT BY CALCULUS OF VARIATIONS

The equation of motion along the flight path (see sketch (a))

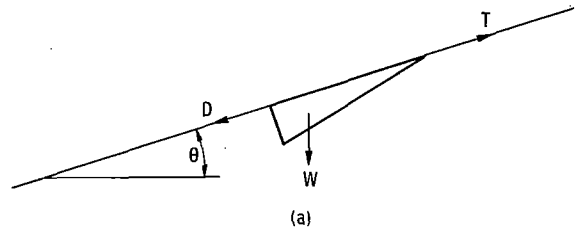

(a)

is

$$T - D - W \sin \theta = \frac{W}{g} \frac{dV_o}{dt}$$

Rearranging the equation gives

$$\frac{T}{W} = \frac{\sin \theta + \frac{1}{g} \frac{dV_o}{dt}}{1 - \frac{D}{T}}$$

However, the thrust is given by

$$T = \frac{dW}{dt} I_s$$

Hence, the previous equation can be put in the form

$$\frac{dW}{W} = \frac{1}{I_s} \frac{\sin \theta \, dt + dV_o/g}{1 - \frac{D}{T}} \tag{A1}$$

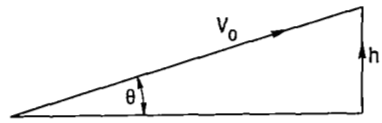

(b)

As shown in sketch (b), $\dot{h} = V_o \sin\theta$ or

$$\sin\theta \, dt = \frac{\dot{h}}{V_o} dt = \frac{dh}{V_o}$$

Substituting the previous equation into equation (A1) yields

$$\frac{dW}{W} = \frac{1}{I_s V_o} \frac{1 + \frac{1}{2g}\frac{dV_o^2}{dh}}{1 - \frac{D}{T}} dh$$

$$\int_o^f \frac{dW}{W} = \ln \frac{W_f}{W_o} = \int \frac{1}{I_s V_o} \frac{1 + \frac{1}{2g}\frac{dV_o^2}{dh}}{1 - \frac{D}{T}} dh$$

Hence, to minimize fuel consumption, the following integral has to be maximized:

$$\int \frac{1}{I_s V_o} \frac{1 + \frac{1}{2g}\frac{dV_o^2}{dh}}{1 - \frac{D}{T}} dh = \int F\left(h, V_o^2, \frac{dV_o^2}{dh}\right) dh$$

The Euler-Lagrange equation is

$$\frac{d}{dh}\left(\frac{\partial F}{\partial \frac{dV_o^2}{dh}}\right) = \frac{\partial F}{\partial V_o^2}$$

Hence, the left side is

$$\frac{d}{dh}\left[\frac{\frac{1}{2g}}{V_o I_s\left(1 - \frac{D}{T}\right)}\right] = \frac{\partial}{\partial h}\left[\frac{\frac{1}{2g}}{V_o I_s\left(1 - \frac{D}{T}\right)}\right] + \frac{\partial}{\partial V_o^2}\left[\frac{\frac{1}{2g}}{V_o I_s\left(1 - \frac{D}{T}\right)}\right]\frac{dV_o^2}{dh}$$

and the right side is

$$\frac{\partial}{\partial V_o^2}\left[\frac{1}{V_o I_s\left(1 - \frac{D}{T}\right)}\right] + \frac{\partial}{\partial V_o^2}\left[\frac{\frac{1}{2g}\frac{dV_o^2}{dh}}{V_o I_s\left(1 - \frac{D}{T}\right)}\right]$$

Equating and simplifying give

$$\frac{\partial}{\partial h}\left[V_o I_s\left(1 - \frac{D}{T}\right)\right] = \frac{2g\partial}{\partial V_o^2}\left[V_o I_s\left(1 - \frac{D}{T}\right)\right] \tag{A2}$$

Thus, the function to be examined can be expressed in terms of airplane and propulsion parameters

$$\frac{V_o I_s}{T}(T - D) = \frac{V_o(T - D)}{m_1 \frac{f}{a}} \tag{A3}$$

for the general case of a scramjet since

$$T = m_1 \frac{f}{a} I_s$$

The overall efficiency of the powerplant, which is relatively constant in the hypersonic region, is defined as

$$\eta_{oa} = \frac{TV_o}{fQJ}$$

and thus

$$\frac{TV_o}{m_1} = \eta_{oa} \frac{f}{a} JQ$$

If Newtonian flow is assumed, the aerodynamic lift coefficient is

$$C_L \simeq C_N = 2 \sin^2 \alpha \simeq \frac{W(1 - \overline{V}^2)}{qS}$$

from which

$$\alpha \approx \sqrt{\frac{W(1 - \overline{V}^2)}{2qS}}$$

and further, the drag due to lift coefficient is

$$(C_D)_i = 2 \sin^3 \alpha \approx 2\alpha^3 \approx 2\left[\frac{W(1 - \overline{V}^2)}{2qS}\right]^{3/2}$$

So the total drag including friction is

$$D = D_i + D_f = \left\{\left[\frac{W(1 - \overline{V}^2)}{\rho V_o^2 S}\right]^{3/2} + \frac{(C_D)_f}{2}\right\} \rho V_o^2 S$$

Since $m_1 = \rho V_o A_{oo}$,

$$\frac{(T - D)V_o}{m_1} = \eta_{oa} \frac{f}{a} JQ - \frac{\left[W(1 - \bar{V}^2)\right]^{3/2}}{\rho^{3/2} S^{1/2} V_o A_{oo}} - \frac{(C_D)_f}{2} V_o^2 \frac{S}{A_{oo}}$$

Differentiating the previous equation with respect to h and V_o^2 yields

$$\frac{\partial \dfrac{(T - D)V_o}{m_1}}{\partial h} = \frac{3}{2} \frac{\left[W(1 - \bar{V}^2)\right]^{3/2}}{\rho^{5/2} S^{1/2} A_{oo} V_o} \frac{d\rho}{dh} \tag{A4}$$

$$\frac{\partial}{\partial V_o^2}\left[\frac{(T - D)V_o}{m_1}\right] = \frac{3}{2} \frac{W^{3/2}\left(1 - \bar{V}^2\right)^{1/2}}{V_o \rho^{3/2} S^{1/2} V_r^2 A_{oo}} + \frac{1}{2} \frac{W^{3/2}\left(1 - \bar{V}^2\right)^{3/2}}{\rho^{3/2} S^{1/2} A_{oo} V_o^3} - \frac{(C_D)_f}{2} \frac{S}{A_{oo}} \tag{A5}$$

Substituting equations (A3), (A4), and (A5) into (A2) yields

$$\frac{d\rho}{dh} = \left(\frac{2g}{V_r^2 - V_o^2} + \frac{2}{3} \frac{g}{V_o^2}\right)\rho - \frac{2}{3} g \frac{(C_D)_f V_o S^{3/2}}{\left[W(1 - \bar{V}^2)\right]^{3/2}} \rho^{5/2} \tag{A6}$$

The form of equation (A6) is

$$\frac{d\rho}{dh} = a_1 \rho - b_1 \rho^{5/2} \tag{A7}$$

Using $\rho = X^2$ and $d\rho = 2X\, dX$ gives

$$\frac{dX}{X\left(a_1 - b_1 X^3\right)} = \frac{dh}{2} \tag{A8}$$

which can be integrated directly tc give

$$X^3 = \frac{a_1}{b_1 + K_1^3 \exp\left(-\frac{3}{2} a_1 h\right)} \tag{A9}$$

Returning to the original notation of equation (A6) gives

$$a_1 = \frac{2g}{3V_o^2}\left(\frac{3\bar{V}^2}{1 - \bar{V}^2} + 1\right)$$

$$b_1 = \frac{2g}{3}\,\frac{(C_D)_f S^{3/2} V_o}{\left[W(1 - \bar{V}^2)\right]^{3/2}}$$

and equation (A9) becomes

$$\rho^{3/2} = \frac{\left(\frac{3\bar{V}^2}{1 - \bar{V}^2} + 1\right)}{(C_D)_f \frac{S^{3/2} V_o^3}{\left[W(1 - \bar{V}^2)\right]^{3/2}} + \frac{K_1}{2g} 3V_o^2 \exp\left[-\frac{3}{2} h \frac{2g}{3V_o^2}\left(\frac{3\bar{V}^2}{1 - \bar{V}^2} + 1\right)\right]} \tag{A10}$$

$$1 = \frac{\left(\frac{3\bar{V}^2}{1 - \bar{V}^2} + 1\right)}{\frac{2D_f}{D_i} + \frac{3K_1}{2g} \rho^{3/2} V_o^2 \exp\left[-\frac{hg}{V_o^2}\left(\frac{3\bar{V}^2}{1 - \bar{V}^2} + 1\right)\right]}$$

For the initial part of the trajectory, $D_f << D_i$ ($D_i \approx 12D_f$ at $M_s = 10$), and therefore

$$\frac{3}{2g} K_2 \rho^{3/2} V_o^2 = K_3 \exp\left(\frac{hg}{V_o^2} K_3\right) \tag{A11}$$

where

$$K_3 = \frac{3\bar{V}^2}{1 - \bar{V}^2} + 1$$

For the region of the trajectory where $hg/V_o^2 \ll 1$ and $\overline{V}^2 \ll 1$,

$$\rho^{3/2} V_o^2 = \text{Constant}$$

or

$$pM^{4/3} = \text{Constant}$$

In the region near $\overline{V} \rightarrow 1.0$, $D_f \approx D_i$ and the constant increases greatly, which means the trajectory would be required to dip steeply to lower altitudes or higher pressure. Actually, it is indeterminate at the $\overline{V} = 1.0$ condition. The associated power requirements preclude the adoption of such a trajectory. Therefore, in the interest of simplicity, the path or trajectory defined by a constant product of atmospheric pressure and flight Mach number (pM = Constant) has been used from the staging point to the zoom velocity.

This assumption has the advantage of giving nearly constant mass flow rate ($m_1 \propto 1/\sqrt{t_o}$, where t_o is the ambient temperature) and fuel flow rate since the fuel-air ratio is also a constant. A comparison of paths characterized by constant pM, $pM^{4/3}$, or the commonly used constant dynamic pressure pM^2 is given in figure 3.

APPENDIX B

PULLUP MANEUVER

The flight path sequence between the attainment of zoom velocity and orbit conditions is depicted in sketch (c). The velocity at the end of the acceleration flight path is denoted

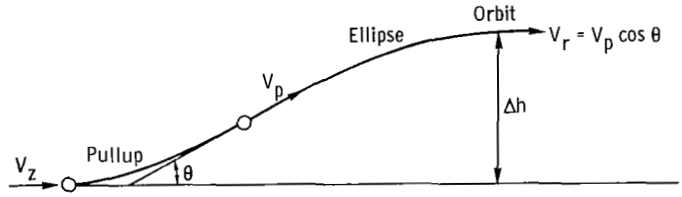

(c)

by V_z. This is the speed with which the pullup is initiated. During the pullup the equations of motion neglecting gravity are

$$L = mV^2 \frac{d\theta}{dS}$$

$$-D = m \frac{dV}{dt}$$

Dividing one equation by the other and noting that $dS/dt = V$ give

$$\frac{L}{D} \frac{dV}{V} = -d\theta$$

Integration of this equation yields

$$V_p = V_z \exp\left(-\frac{\theta}{L/D}\right) \tag{B1}$$

Subsequent to the pullup, the equation of motion is

$$\ddot{h} = -g$$

Integration gives

$$\dot{h} = V_z \exp\left(-\frac{\theta}{L/D}\right)\sin\theta - gt$$

and

$$h = V_z \exp\left(-\frac{\theta}{L/D}\right)t \sin\theta - \frac{1}{2}gt^2$$

At the peak of the free flight, $\dot{h} = 0$; hence,

$$t = \frac{V_z \exp\left(-\frac{\theta}{L/D}\right)\sin\theta}{g}$$

Substituting this expression for t in the expression for h yields

$$h = \frac{1}{2}\frac{\left[V_z \exp\left(-\frac{\theta}{L/D}\right)\sin\theta\right]^2}{g}$$

At the peak,

$$V_z \exp\left(-\frac{\theta}{L/D}\right)\cos\theta = V_r \tag{B2}$$

Hence,

$$h = \frac{1}{2}\frac{\left(V_r \tan\theta\right)^2}{g}$$

Thus,

$$\tan^2\theta = \frac{2gh}{V_r^2} \tag{B3}$$

The following can be substituted into equations (B1) to (B3): $h = 100$ miles (1.6×10^5 m), $V_r = 26\,000$ ft/sec (7925 m/sec), $\theta = 12.6^\circ$, and relations are obtained for V_p and V_z as functions of L/D.

APPENDIX C

HYBRIDIZATION OF ENGINES

The hybridization of powerplants leads in principle to an advantage over their separate, though simultaneous, use. In the case of a hybrid, the total enthalpy of the mixed flow is the sum of the total enthalpies of the rocket flow and the airflow, which, per unit mass of mixed flow, becomes

$$\frac{\overline{m}\left(h_1^o + Q\right) + h_j^o}{\overline{m} + 1}$$

and the gross jet thrust obtained per unit mass of rocket flow is proportional to

$$(\overline{m} + 1)\sqrt{\frac{\overline{m}\left(h_1^o + Q\right) + h_j^o}{\overline{m} + 1}}$$

In the case of a two-ducted system, the gross jet thrust of the scramjet is proportional to

$$m_1\sqrt{h_1^o + Q}$$

and the gross jet thrust of the rocket is

$$m_j\sqrt{h_j^o}$$

The total thrust of the two systems mounted together per unit mass of rocket flow is

$$\overline{m}\sqrt{h_1^o + Q} + \sqrt{h_j^o}$$

If it is assumed that the hybrid is superior, the following inequality is obtained:

$$(\overline{m} + 1)\sqrt{\frac{\overline{m}\left(h_1^o + Q\right) + h_j^o}{\overline{m} + 1}} \geq \overline{m}\sqrt{h_1^o + Q} + \sqrt{h_j^o}$$

Squaring both sides yields

$$(\overline{m} + 1)\left[\overline{m}\left(h_1^o + Q\right) + h_j^o\right] \geq \overline{m}^2\left(h_1^o + Q\right) + h_j^o + 2\overline{m}\sqrt{h_1^o + Q}\sqrt{h_j^o}$$

Simplifying gives

$$h_1^o + Q + h_j^o \geq 2\sqrt{h_1^o + Q}\sqrt{h_j^o}$$

or

$$\left(\sqrt{h_1^o + Q} - \sqrt{h_j^o}\right)^2 \geq 0$$

Since the square of a number is always positive, the inequality is always satisfied. Hence, the hybrid system is, in general, superior to the separate system. However, at very high velocities the sum $h_1^o + Q$, which is total enthalpy of inducted air plus heat added to it, becomes not much different in magnitude from the total enthalpy of the rocket h_j^o. The inequality turns into the equality. Thus, in the hypersonic region of flight the benefits of hybridization are largely lost.

APPENDIX D

AERODYNAMIC CHARACTERISTICS OF THE VEHICLE

Expressions for the lift, drag, and lift-drag ratio are derived for a somewhat simplified model of the prismatic-delta vehicle illustrated in figure 2. A further simplification is the use of Newtonian impact theory.

The vehicle shown in sketch (d) in horizontal flight is at an angle of attack designated

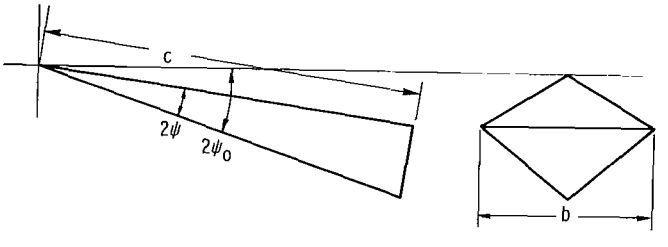

(d)

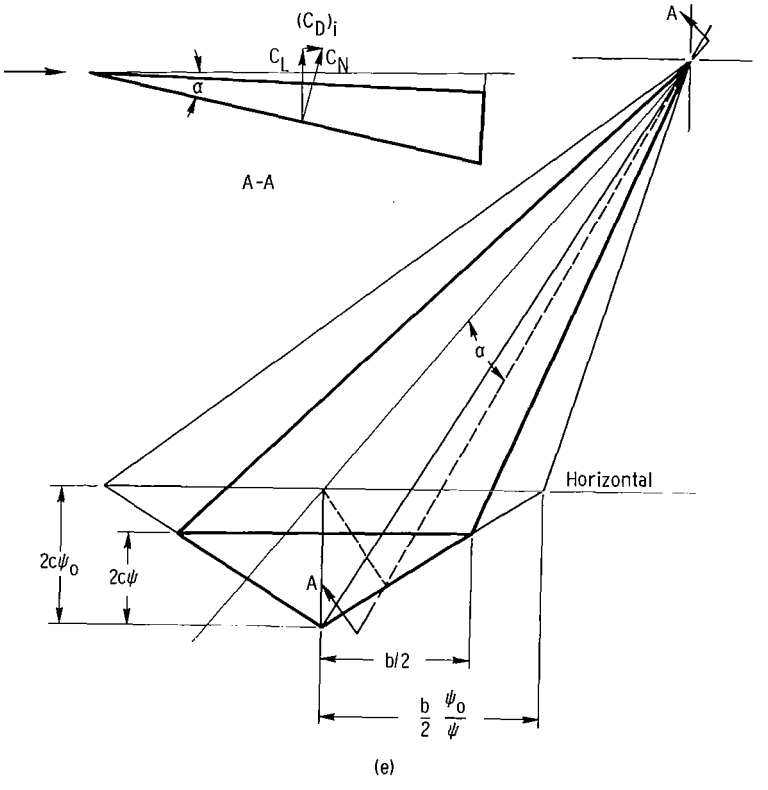

(e)

as $2\psi_o$ and has a wedge angle at the centerline of 2ψ, both defined in the vertical plane of symmetry.

The starboard-rear view of the vehicle is shown in sketch (e). The configuration outline is shown by the bold lines, whereas the effective configuration simulated at angle of attach is shown by the light outline. Because the bottom lifting surface is skewed to the coordinate system, the usual Newtonian parameters must be converted to the coordinate axies.

Section A-A of sketch (e) taken normal to the bottom impact surface simulates a flat plate at angle of attack α and the usual Newtonian relations apply and are listed as follows:

$$C_N = 2 \sin^2\alpha = C_p$$

$$C_L = 2 \sin^2\alpha \cos \alpha$$

$$(C_D)_i = 2 \sin^3\alpha$$

Using the similarity of triangles at the base of the vehicle (see sketch (f))

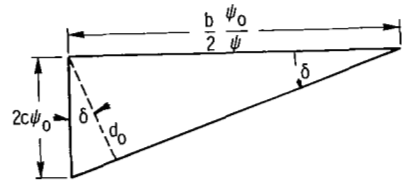

(f)

gives

$$\cos \delta = \frac{d_o}{2c\psi_o} = \frac{\frac{b}{2}\frac{\psi_o}{\psi}}{\sqrt{\left(\frac{b}{2}\frac{\psi_o}{\psi}\right)^2 + (2c\psi_o)^2}} = \frac{1}{\sqrt{1 + \left(\frac{4\psi}{b/c}\right)^2}} \qquad \text{(D1)}$$

But,

$$\cos \delta = \frac{S_o}{A_o} \frac{\cos(2\psi_o - 2\psi)}{\cos 2\psi} \qquad \text{(D2)}$$

where the planform area of the effective wedge is

$$S_o = \frac{b}{2} \frac{\psi_o}{\psi} \frac{c}{\cos(2\psi_o - 2\psi)}$$

The bottom surface area of the effective wedge is

$$A_o = \frac{c}{\cos 2\psi} \sqrt{\left(\frac{b}{2} \frac{\psi_o}{\psi}\right)^2 + (2c\psi_o)^2}$$

Resolving the normal force coefficient to the vertical plane (see sketch (g))

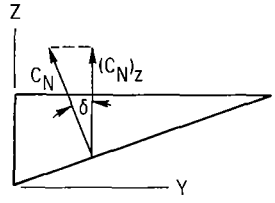

(g)

gives

$$(C_N)_Z = C_N \cos \delta = C_N \frac{S_o}{A_o} \frac{\cos(2\psi_o - 2\psi)}{\cos 2\psi}$$

Converting to the lift coefficient in the vertical plane yields

$$C_L = (C_N)_Z \cos 2\psi_o = C_N \frac{S_o}{A_o} \frac{\cos 2\psi_o \cos(2\psi_o - 2\psi)}{\cos 2\psi}$$

or, approximately,

$$C_L \simeq C_N \frac{S_o}{A_o} \tag{D3}$$

Now

$$\frac{L}{q} = C_N A \frac{S_o}{A_o} = C_N \frac{A}{A_o} \frac{S_o}{S} S$$

and since

$$\frac{S_o}{S} = \frac{\left(\frac{b}{2}\right)\frac{\psi_o}{\psi} \frac{c}{\cos(2\psi_o - 2\psi)}}{\frac{bc}{2}} = \frac{\psi_o}{\psi \cos(2\psi_o - 2\psi)} \simeq \frac{\psi_o}{\psi}$$

and

$$\frac{A_o}{A} = \frac{\sqrt{\left(\frac{b}{2}\frac{\psi_o}{\psi}\right)^2 + (2c\psi_o)^2} \frac{c}{\cos 2\psi}}{\sqrt{\left(\frac{b}{2}\right)^2 + (2c\psi)^2} \frac{c}{\cos 2\psi}} \simeq \frac{\psi_o}{\psi}$$

therefore, approximately,

$$\frac{L}{q} \simeq C_N S \tag{D4}$$

The drag due to lift can now be evaluated:

$$(C_D)_i = C_L \tan 2\psi_o$$

$$\tan 2\psi_o = 2\psi_o \cos(2\psi_o - 2\psi)$$

Then using C_L from equation (D3) gives

$$(C_D)_i \simeq C_N \frac{S_o}{A_o} 2\psi_o$$

and, approximately,

$$\frac{D_i}{q} = C_N \frac{A}{A_o} \frac{S_o}{S} S2\psi_o \simeq C_N 2\psi_o S \tag{D5}$$

In order to evaluate the friction drag the outside area is found (see sketch (h)):

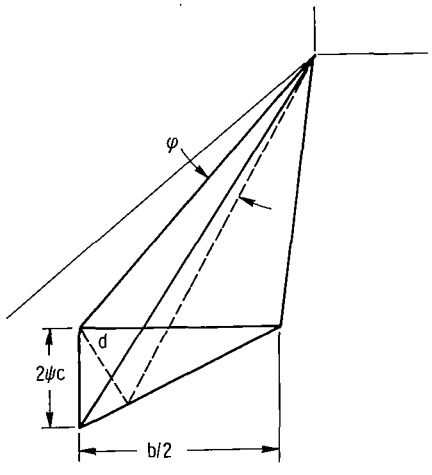

(h)

$$c \tan \varphi = d = \frac{2\psi c(b/2)}{\sqrt{(2\psi c)^2 + (b/2)^2}}$$

$$\tan \varphi = \frac{\psi b}{\sqrt{(2\psi c)^2 + (b/2)^2}}$$

$$\frac{1}{\cos^2 \varphi} = \frac{(2\psi c)^2 + (b/2)^2 + (\psi b)^2}{(2\psi c)^2 + (b/2)^2}$$

Hence, the under surface of the wedge is

$$\frac{A}{2} = \frac{c}{2} \sqrt{\left(\frac{b}{2}\right)^2 + (2\psi c)^2} \sqrt{\frac{(2\psi c)^2 + (b/2)^2 + (\psi b)^2}{(2\psi c)^2 + (b/2)^2}}$$

Since

$$\frac{S}{2} = \frac{1}{2}\,\frac{bc}{2}$$

therefore

$$\frac{A}{S} = \sqrt{1 + (2\psi)^2 + \left(\frac{4\psi}{b/c}\right)^2} \tag{D6}$$

Now the friction drag to dynamic pressure ratio will be

$$\frac{D_f}{q} = C_f(A + S) = C_f\left(\frac{A}{S} + 1\right)S = C_f\,\frac{bc}{2}\left[1 + \sqrt{1 + (2\psi)^2 + \left(\frac{4\psi}{b/c}\right)^2}\right]$$

The lift-drag ratio can be written

$$\frac{L}{D} = \frac{C_N S}{C_N S 2\psi_o + C_f S\left[1 + \sqrt{1 + (2\psi)^2 + \left(\frac{4\psi}{b/c}\right)^2}\right]}$$

and from previous geometry

$$\frac{C_N}{2} = \sin^2\alpha = \frac{1}{1 + \dfrac{1 + \left(\dfrac{4\psi}{b/c}\right)^2}{4\psi_o^2}} \tag{D7}$$

The lift-drag ratio in terms of ψ_o, ψ, b/c, and C_f is then, when $\psi_o > \psi$,

$$\frac{L}{D} = \frac{1}{2\psi_o + \dfrac{C_f}{2}\left[1 + \sqrt{1 + (2\psi)^2 + \left(\dfrac{4\psi}{b/c}\right)^2}\right]\left\{1 + \left[\dfrac{1 + \left(\dfrac{4\psi}{b/c}\right)^2}{4\psi_o^2}\right]\right\}} \tag{D8}$$

For the prismatic-delta vehicle, the following relation derived from geometry is helpful in relating the basic vehicle parameters for calculations:

$$\frac{V^{2/3}}{S}\left(\frac{b}{c}\right)^{1/3} = \left(\frac{2\sqrt{2}}{3}\psi\right)^{2/3} \tag{D9}$$

Condition for Zero Lift and Angles of Attack Smaller Than Wedge Angle

Aerodynamic lift diminishes as the vehicle accelerates along the climb path and centrifugal lift increases (see fig. 4). Consequently, the angle of attack decreases as orbital speed is approached. For the condition where the angle of attack is less than the wedge angle (see sketch (i)), the negative lift and drag due to lift from the top surface must be found.

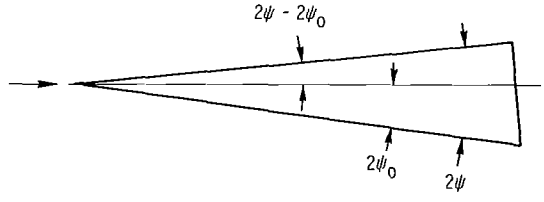

(i)

For the top surface,

$$\left(\frac{L}{q}\right)_{top} = 2S \sin^2 2(\psi - \psi_0)\cos 2(\psi - \psi_0) = 8S \sin^2(\psi - \psi_0)\cos^2(\psi - \psi_0)\cos 2(\psi - \psi_0) \tag{D10}$$

$$\left(\frac{D_i}{q}\right)_{top} = 2S \sin^3 2(\psi - \psi_0) = 16S \sin^3(\psi - \psi_0)\cos^3(\psi - \psi_0) \tag{D11}$$

then

$$\frac{L}{D} = \frac{L_{bottom} - L_{top}}{(D_i)_{bottom} + (D_i)_{top} + D_f}$$

$$\frac{L}{D} = \frac{C_N - 8\sin^2(\psi - \psi_o)\cos^2(\psi - \psi_o)\cos 2(\psi - \psi_o)}{2\psi_o C_N \cos(\psi - \psi_o) + 16\sin^3(\psi - \psi_o)\cos^3(\psi - \psi_o) + C_f\left[1 + \sqrt{1 + (2\psi)^2 + \left(\frac{4\psi}{b/c}\right)^2}\right]} \tag{D12}$$

or

$$\frac{L}{D} \approx \frac{C_N - 8\sin^2(\psi - \psi_o)}{2\psi_o C_N + 16\sin^3(\psi - \psi_o) + C_f(1 + A/S)} \tag{D13}$$

(C_N is found from eq. (D7).)

For the condition of zero net lift,

$$C_N = 8\sin^2(\psi - \psi_o) \tag{D14}$$

This equation is solved for angle of attack which is given the special designation $2\psi_{oo}$.

Determination of Capture Area

An arbitrary rule adopted for sizing the capture area was to limit the span of the inlet area at the condition for zero lift. Hence, at the effective wedge angle giving equal lift on the top and bottom, only the trailing edge of the base remaining below the horizontal was assumed to have inlet capture area (see sketch (j)). The stream tube area is equivalent to the base area below the horizontal axis. This procedure restricts the engine size but avoids the problems of hybrid engine installation near the tip regions, such as the required mixing length and the nozzle-base integration problems.

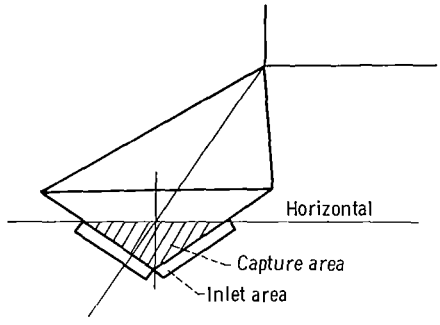

(j)

Alternate assumptions were not evaluated. However, some trade-off between propellant consumption and engine weight due to engine size selection might occur. Thus, a larger size would provide greater thrust during the acceleration phase at the expense of spillage drag (or variable geometry) near the zero lift or orbital condition.

APPENDIX E

STRUCTURAL ANALYSIS

The structural configuration chosen features as a primary element a statically determinate, pin-jointed multiple truss arrangement protected by an insulating skin system. One truss of this scheme is depicted in sketch (k).

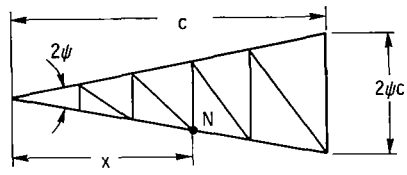

(k)

The truss load is derived by assuming it to be the main supporting structure for the aerodynamic load occurring on a prism of 2ψ wedge angle and 2ϵ vertex angle as shown in sketch (l). Thus, the whole vehicle includes a series of trusses joined at the vertex and separated by an angle 2ϵ, which may vary from truss to truss.

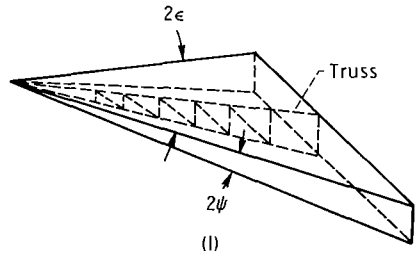

(l)

With a uniform pressure p at the bottom surface of the prismatic wedge, the moment of the forces about a point N, at the distance X from the vertex is

$$M = p\frac{1}{2}(2\epsilon X)X\frac{X}{3} = p\epsilon\frac{X^3}{3}$$

The truss consisting of two bays, as shown in sketch (m), is now considered.

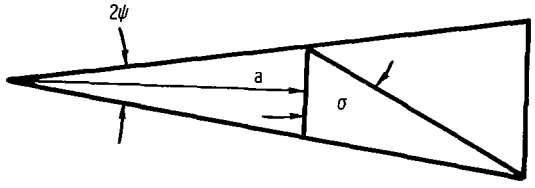

(m)

Its length is approximately

$$a + 2\psi a \tan\sigma = a(1 + 2\psi \tan\sigma)$$

The length of a truss consisting of three bays (see sketch (n))

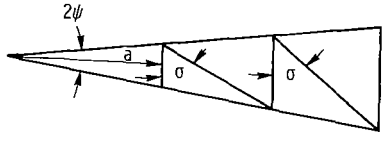

(n)

will be

$$a(1 + 2\psi \tan\sigma) + a(1 + 2\psi \tan\sigma)2\psi \tan\sigma = a(1 + 2\psi \tan\sigma)^2$$

Thus, a truss of n bays will have the length

$$a(1 + 2\psi \tan\sigma)^{n-1}$$

Next is considered the $(n+1)^{th}$ bay with the loading on the truss as shown in sketch (o) where the compression member C, the tension member T, the diagonal member D, and the strut S are identified.

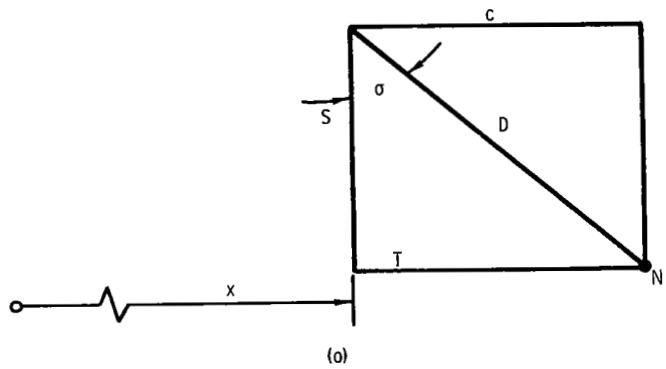

(o)

Cutting a section through the bay and taking moments about the point N give

$$p\epsilon \frac{X^3}{3} = (X + 2\psi X \tan \sigma)2\psi c$$

or

$$p\epsilon \frac{X^2}{3} = (1 + 2\psi \tan \sigma)2\psi c$$

But $C = A_c(f_c)_1$; hence,

$$A_c = p\epsilon \frac{X^2}{3} \frac{1}{(1 + 2\psi \tan \sigma)2\psi} \frac{1}{(f_c)_1}$$

and the volume of the member C is

$$pa^3 \frac{\epsilon}{3} \frac{(1 + 2\psi \tan \sigma)^{3n-4}}{(f_c)_1} \tan \sigma$$

Summing up the volume of all the elements like C gives

$$p\frac{\epsilon}{3}\frac{a^3}{(f_c)_1}\tan\sigma\frac{1}{1+2\psi\tan\sigma}\sum_{j=1}^{n}(1+2\psi\tan\sigma)^{3(j-1)}$$

$$=\frac{p\epsilon}{3}\frac{a^3}{(f_c)_1}\tan\sigma\frac{1}{1+2\psi\tan\sigma}\frac{(1+2\psi\tan\sigma)^{3n}-1}{(1+2\psi\tan\sigma)^3-1}\sim\frac{p\epsilon}{\psi}\frac{1}{18}\frac{c^3}{(f_c)_1}$$

Considering, in turn, the member S and its load gives

$$S=p\frac{1}{2}X(2\epsilon X)=p\epsilon X^2$$

Then the volume of the member S is

$$p\frac{2X^3\epsilon\psi}{(f_c)_2}$$

The summation of the volume of all the struts S is

$$p\frac{2\epsilon\psi}{(f_c)_2}\sum X^3=p\frac{2\epsilon\psi}{(f_c)_2}\sum_{j=1}^{n}a^3(1+2\psi\tan\sigma)^{3(j-1)}$$

$$=p\frac{2\epsilon\psi a^3}{(f_c)_2}\frac{(1+2\psi\tan\sigma)^{3n}-1}{(1+2\psi\tan\sigma)^3-1}\sim\frac{1}{3}\frac{p\epsilon c^3}{(f_c)_2\tan\sigma}$$

The load for the diagonal D is given by

$$D=\frac{pX^2\epsilon}{\cos\sigma}$$

Hence,

$$A_D=\frac{pX^2\epsilon}{f_t\cos\sigma}$$

Thus, the volume of all the elements like D is given by

$$a^3 \frac{p\epsilon}{f_t \cos^2\sigma} \frac{(1 + 2\psi \tan\sigma)^{3n} - 1}{(1 + 2\psi \tan\sigma)^3 - 1} \sim p \frac{1}{3} \frac{\epsilon c^3}{f_t \cos\sigma \sin\sigma}$$

Summing the volume of all the structural material in the truss, the following is obtained:

$$\frac{p\epsilon c^3}{3} \left[\frac{1}{3\psi(f_c)_1} + \frac{1}{(f_c)_2 \tan\sigma} + \frac{1}{f_t \cos\sigma \sin\sigma} \right]$$

where the volume of T has been assumed to be equal to that of C. Volume enclosed by the prism associated with the truss is $(4/3)\epsilon\psi c^3$.

Hence, the volume of the structural material per unit volume of the vehicle is

$$\frac{p}{4\psi} \left[\frac{1}{3\psi(f_c)_1} + \frac{1}{(f_c)_2 \tan\sigma} + \frac{1}{f_t \cos\sigma \sin\sigma} \right]$$

Minimization of this quantity with respect to σ reveals $\sigma \sim 45^\circ$.

Then, $p = 2(2\psi)^2 q$ is substituted for the condition of maximum L/D during the pullup into orbit, and ρ_{ss} is defined as the density of stainless steel. The trusswork weight per unit volume is

$$\rho_T = K \frac{\rho_{ss} 2(2\psi)^2 q}{4\psi} \left[\frac{1}{3\psi(f_c)_1} + \frac{1}{(f_c)_2} + \frac{2}{f_t} \right]$$

Selecting values of $(f_c)_1$, $(f_c)_2$, and f_t for stainless steel at mild temperatures and an appropriate constant K results in the variation of trusswork density with dynamic pressure as shown in figure 13. Instability or buckling of the thin-walled structural members was not considered in this initial analysis; however, some adjustment of the estimated trusswork density can be provided by the constant K.

APPENDIX F

CALCULATION PROCEDURE

The following dependent parameters are selected:

(1) A range of values of $V^{2/3}/S$ with b/c corresponding to maximum L/D as given in figure 9 (p. 12)

(2) A flight path constant such as $pM = 0.1$ atmosphere

(3) A range of air-augmentation ratios $\overline{m}$

(4) A range of volumes V or initial weight W_o

The associated wedge angle 2ψ can be found by using equation (D9). The angle of attack for zero net lift $2\psi_{oo}$ is found from

$$L = \left[C_N - 8 \sin^2(\psi - \psi_o)\right] qS \tag{F1}$$

The capture area determined at the zero lift condition as defined in appendix D is

$$A_{oo} = V^{2/3} \left(\frac{2\psi_{oo}}{2\psi}\right)^2 \frac{2\psi}{\frac{V^{2/3}}{S}} \tag{F2}$$

The ratio of tail or afterbody to front or wedge volume for the 45^o boattail angle shown in figure 2 (p. 4) is equal to 2ψ; hence, the total volume is

$$V_T = (1 + 2\psi)V \tag{F3}$$

Now the empty stage weight W_S can be found since the densities and unit weights are known for

$$W_S = K_4 \left[V_T(\rho_T + \rho_t) + A_{oo}\rho_E + 0.37 \frac{A_{oo} pM_o}{\overline{m}} + S_{oa}\rho_s\right] \tag{F4a}$$

or for the pure rocket

$$W_S = K_4 \left[V_T(\rho_T + \rho_t) + 7.9\, m_j + S_{oa}\rho_s\right] \tag{F4b}$$

where

ρ_T weight of trusswork per unit enclosed volume (see fig. 13)

ρ_t tanks, 1.0 lb/ft^3 (16 kg/m^3)

ρ_E secondary component weight, 50 lb/ft^2 (244 kg/m^2)

ρ_s skin, function of temperature (see fig. 12) on a given path

K_4 adjusting constant (landing equipment, etc.), usually 1.2

The propellant density of hydrogen and oxygen for the rocket and hydrogen for the air is combined in a single number according to the air-augmentation ratio as listed in table II. The total propellant weight is initially estimated as

$$W_F = \rho_f V \tag{F5}$$

This corresponds to filling the front prismatic wedge with propellant and having the tail or afterbody volume or its equivalent for other equipment, etc.

When the payload P is specified, the stage weight can be found:

$$W_o = W_S + W_F + P \tag{F6}$$

Now, the performance along the flight path can be determined starting at the staging Mach number. The required lift coefficient (approximate normal force) is

$$C_N = 2 \sin^2 \alpha = \frac{W_o(1 - \overline{V}^2)}{qS} \tag{F7}$$

If $\psi_o \leq \psi$, equation (F1) is used.

Equation (D7) is used to find the angle of attack $2\psi_o$ and then the instantaneous L/D is found from equation (D8) when $\psi_o > \psi$ or equation (D13) if $\psi_o \leq \psi$.

The thrust can be found since the impulse I_s is a function of V_o, $\overline{m}$, and m_1, and the fuel-air ratio is 0.029.

$$T = m_1\left(\frac{1}{\overline{m}} + \frac{f}{a}\right)I_s \tag{F8}$$

The change in weight with velocity is given by equation (F9), which is numerically integrated between the desired velocity limits following the procedure outlined previously:

$$\frac{dW}{dV_o} = -\frac{W}{gI_s} \frac{1 + \frac{g}{V_o} \frac{dh}{dV_o}}{1 - \frac{D}{T}} \tag{F9}$$

The final velocity is determined by the maximum L/D (see fig. 5, p. 7). The total propellant weight determined by equation (F9) is compared with the estimate of equation (F5), the estimate is revised, and the calculation repeated until the iteration converges. An optimum payload to initial weight ratio P/W_o can be found by calculating a range of volumes.

APPENDIX G

SYMBOLS

A	bottom surface area of wedge
A_o	bottom surface area of simulated wedge
A_{oo}	capture area of engine (established at angle of attach for L/D = 0, see appendix D)
$A_{oo}/V^{2/3}$	capture area-volume parameter
a	length of body in truss
a_1	mathematical constant
b	vehicle span
b/c	span to length ratio
b_1	mathematical constant
$(C_D)_f$	friction drag coefficient
$(C_D)_i$	drag due to lift coefficient
C_F	specific thrust coefficient, T/qA_{oo}
C_f	coefficient of friction
C_L	lift coefficient
C_N	normal force coefficient
$(C_N)_Z$	normal force coefficient in Z-direction
c	vehicle length or chord (front wedge)
D	drag
D_f	friction drag
D_i	drag due to lift
d	length
F	function
f	fuel flow rate, lb mass/sec; kg/sec
f/a	fuel-air ratio
$(f_c)_1$	allowable compressive stress
$(f_c)_2$	allowable compressive stress
f_t	allowable tensile stress
g	acceleration due to gravity
h	altitude
h_j^o	stagnation enthalpy of rocket flow
h_m^o	stagnation enthalpy of mixed flow
h_1^o	stagnation enthalpy of air flow (secondary)
I_s	specific impulse, sec
J	mechanical equivalent of heat, 778 ft-lb/Btu; 4186 J/kg-cal
$K, K_{1,2,3,4}$	mathematical constants
L	lift
L/D	lift-drag ratio
M, M_o	flight Mach numbers
M_s	staging Mach number
m	vehicle mass
$\overline{m}$	air-augmentation ratio, $\frac{\text{air flow}}{\text{rocket flow}} = \frac{m_1}{m_j}$

m_j	rocket flow, lb mass/sec; kg/sec
m_1	secondary flow (air), lb mass/sec; kg/sec
P	payload
p	pressure
Q	heat added, Btu/lb air; cal/kg
q	dynamic pressure, $(\gamma/2)\ pM^2$
S	planform area of vehicle
S_o	planform area of simulated wedge
S_{oa}	total outside area of vehicle (skin), S + A
$S_{oa}/V^{2/3}$	skin area-volume parameter
s	path distance
T	vehicle thrust
t	time, sec
t_1	thickness
V	volume
$\overline{V}$	ratio of flight to orbital velocity, V_o/V_r
V_o	flight velocity
V_p	velocity at end of pullup
V_r	orbital velocity, 26 000 ft/sec; 7925 m/sec
V_T	total volume of vehicle
V_z	zoom velocity (at end of powered path and at beginning of pullup)
V_3	jet velocity
$V^{2/3}/S$	volume-surface parameter
W	instantaneous vehicle weight
W_F	propellant weight
W_o	initial vehicle weight
W_{oa}	skin weight
W_S	empty weight
X	distance
α	equivalent flat-plate angle of attack
β	shock wave angle
γ	ratio of specific heats, C_p/C_v
δ	angle between vertical and normal to wedge lower surface
2ϵ	vertex angle of vehicle
θ	flight path angle
λ	variable
ρ	atmospheric density
ρ_E	weight per unit capture area of airbreathing component
ρ_f	propellant density
ρ_s	unit skin weight
ρ_{ss}	density of stainless steel
ρ_T	trusswork density
ρ_t	propellant tank density
σ	angle between vertical and diagonal truss members
φ	true wedge angle
2ψ	wedge angle of vehicle in vertical plane (fig. 2)

$2\psi_o$ vehicle angle of attack (fig. 2)

$2\psi_{oo}$ vehicle angle of attack for zero lift

REFERENCES

1. Escher, William J. D.; Flornes, Bruce J.; and Frank, Harry: Results of a Study of Composite Propulsion Systems for Advanced Launch Vehicle Applications. Presented at AIAA Second Propulsion Joint Specialist Conference, Colorado Springs, Colorado, June 13-17, 1966.

2. Vaglio-Laurin, Roberto; and Finke, Reinald G.: Reusable Space Launch Vehicle Concepts - Outlook 1965. Paper No. 650801, SAE, Oct. 1965.

3. Franciscus, Leo C.: Off-Design Performance of Hypersonic Supersonic Combustion Ramjets. Paper No. 64-248, AIAA, July 1964.

4. Dobrowolski, Andrzej: Analysis of Nonconstant Area Combustion and Mixing in Ramjet and Rocket-Ramjet Hybrid Engines. NASA TN D-3626, 1966.

5. Küchemann, D.: Hypersonic Aircraft and Their Aerodynamic Problems Progress in Aeronautical Sciences. Vol. 6. D. Küchemann and L. H. G. Sterne, eds., Pergamon Press, 1965, pp. 271-353.

6. Larson, Howard K.: The Hypersonic Shape. Space/Aeronautics, vol. 44, no. 4, Sept. 1965, pp. 69-75.

7. Alelyunas, Paul: L > D Spacecraft. Space/Aeronautics, vol. 47, no. 2, Feb. 1967, pp. 52-65.

8. Dickson, J.: Thermal Protection with Temperature Capability to 2500^{o} F for Cool Structures. Conference on Aerodynamically Heated Structures, AF Office of Scientific Research and Arthur D. Little, Inc., Cambridge, Mass., July 25-26, 1961.

NASA-Langley, 1969 —— 28 E-4144